Spectroscopic study of the radionuclide ^{21}Na for the astrophysical ^{17}F$(\alpha,p)^{20}$Ne reaction rate

S. M. Cha (차수미),[1] K. Y. Chae (채경육),[1,*] S. Ahn (안성훈),[2] D. W. Bardayan,[3] K. A. Chipps,[4] J. A. Cizewski,[5] M. E. Howard,[5] R. L. Kozub,[6] K. Kwak (곽규진),[7] B. Manning,[5] M. Matos,[8] P. D. O'Malley,[5] S. D. Pain,[9] W. A. Peters,[10] S. T. Pittman,[9] A. Ratkiewicz,[5] M. S. Smith,[9] and S. Strauss[5]

[1]*Department of Physics, Sungkyunkwan University, Suwon 16419, Korea*
[2]*Department of Physics and Astronomy, University of Tennessee, Knoxville, Tennessee 37996, USA*
[3]*Department of Physics, University of Notre Dame, Notre Dame, Indiana 46556, USA*
[4]*Department of Physics, Colorado School of Mines, Golden, Colorado 80401, USA*
[5]*Department of Physics and Astronomy, Rutgers University, New Brunswick, New Jersey 08903, USA*
[6]*Department of Physics, Tennessee Technological University, Cookeville, Tennessee 38505, USA*
[7]*Department of Physics, School of Natural Science, Ulsan National Institute of Science and Technology (UNIST), Ulsan 44919, Korea*
[8]*Department of Physics and Astronomy, Louisiana State University, Baton Rouge, Louisiana 70803, USA*
[9]*Physics Division, Oak Ridge National Laboratory, Oak Ridge, Tennessee 37831, USA*
[10]*Oak Ridge Associated Universities, Oak Ridge, Tennessee 37831, USA*

(Received 28 April 2017; published 31 August 2017)

The ^{24}Mg$(p,\alpha)^{21}$Na reaction was measured at the Holifield Radioactive Ion Beam Facility of the Oak Ridge National Laboratory to study the spectroscopy of the radionuclide ^{21}Na. A 31-MeV proton beam from the 25 MV tandem accelerator bombarded isotopically enriched ^{24}Mg targets. Recoiling ^{4}He particles were identified by an annular silicon strip detector array. Two energy levels at $E_x = 6.594$ and 7.132 MeV were observed for the first time. By comparing the experimentally obtained angular distributions and distorted wave Born approximation calculations, the spins and parities of ^{21}Na energy levels were constrained. The astrophysically-important ^{17}F$(\alpha,p)^{20}$Ne reaction rate was also calculated for the first time using resonance parameters for 12 energy levels.

DOI: 10.1103/PhysRevC.96.025810

I. INTRODUCTION

Observations of the characteristic 1.157 MeV γ rays from the radioactive decay of ^{44}Ti ($t_{1/2} = 59.1$ y) provide an ideal probe for constraining the explosion mechanism of core-collapse supernovae, since the production of the isotope is very sensitive to the temperature, density, and electron fraction evolution of the star [1–7]. As pointed out by Young *et al.* [1], the inferred amount of synthesized mass of ^{44}Ti at the Cassiopeia A remnant is abnormally large compared to spherical explosion model calculations [2]. To address this issue, Magkotsios *et al.* studied the influence of various nuclear reactions on the ^{44}Ti abundance produced from core-collapse supernovae [3]. In their work, various (α,γ), (α,p), (p,γ), (p,α), (p,n), and (α,n) reactions in light and intermediate-mass targets were considered and the variation in the ^{17}F$(\alpha,p)^{20}$Ne reaction rate was found to have a "primary" impact on the ^{44}Ti abundance.

In more recent work by Cyburt *et al.*, the importance of the ^{17}F$(\alpha,p)^{20}$Ne reaction rate was emphasized in relation to its effect on the x-ray burst light curve [8]. The one dimensional multizone hydrodynamics code Kepler [9] and a set of 1931 (p,γ), (α,γ), and (α,p) reaction rates on neutron-deficient isotopes in the nuclear mass range of $A = 1$–106 were used for the sensitivity study on the x-ray light curve and the composition of the burst ashes. Their results indicate that varying the ^{17}F$(\alpha,p)^{20}$Ne reaction rate by a factor of 10 causes significant effects on both the light curve and composition. The ^{17}F$(\alpha,p)^{20}$Ne reaction rate, however, has never been measured and significant uncertainties exist. Because the reaction rate depends upon the properties of ^{21}Na levels located above the α threshold at 6.561 MeV, searching for new energy levels in ^{21}Na and studying their properties may improve our understanding of the abundance of ^{44}Ti and the x-ray burst light curve.

To study the energy levels in ^{21}Na of interest for the ^{17}F$(\alpha,p)^{20}$Ne reaction rate, the ^{24}Mg$(p,\alpha)^{21}$Na reaction was measured at the Holifield Radioactive Ion Beam Facility (HRIBF) at Oak Ridge National Laboratory (ORNL). The ^{24}Mg$(p,\alpha)^{21}$Na reaction has been reported only one time previously, by Pronko *et al.* [10], where only the lower excited states ($E_x < \sim 5$ MeV) of ^{21}Na were investigated. In the present work, the energy levels of ^{21}Na up to ~7.2 MeV were identified, which provides the first spectroscopic results for six energy levels in the energy range of $E_x = 5$–7.2 MeV.

II. EXPERIMENT

The experimental setup is shown in Fig. 1. Proton beams of 31 MeV from the 25 MV electrostatic tandem accelerator were delivered to isotopically enriched (99.9%) ^{24}Mg solid targets with thicknesses of 520 μg/cm^2 and 516 μg/cm^2, respectively. The targets were fabricated by the National Isotope Development Center (NIDC) located at the Oak Ridge National Laboratory. The target material was rolled in a 304 stainless steel rolling pack to the desired thickness. The

*kchae@skku.edu

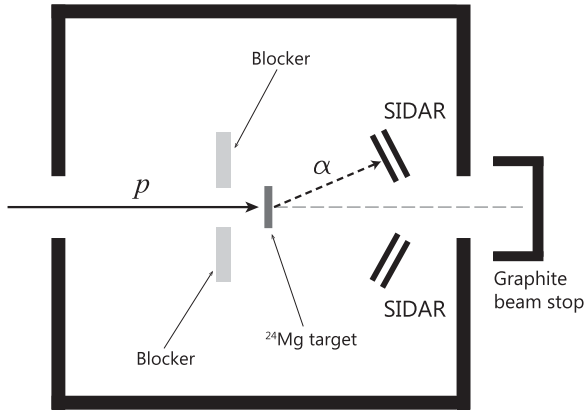

FIG. 1. A schematic diagram of the experimental setup is shown. A 31-MeV proton beam impinged on isotopically enriched ^{24}Mg solid targets. Recoiling α particles were detected at forward angles by the SIDAR. A graphite beam stop was used to monitor the beam current.

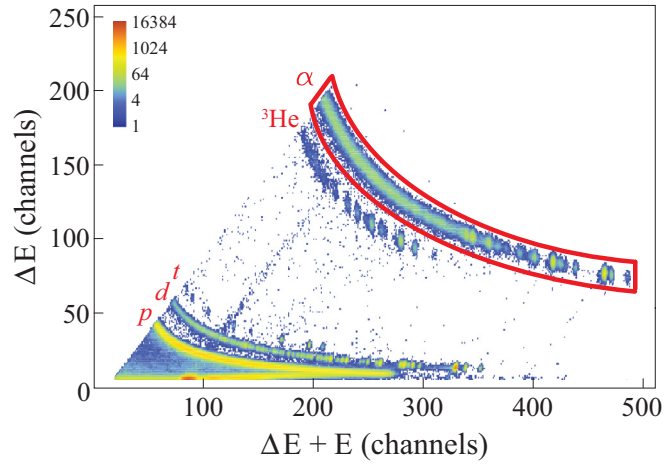

FIG. 2. A typical particle-identification plot is shown. The α particles from the ^{24}Mg$(p,\alpha)^{21}$Na reaction are clearly separated from the other light charged particles such as p,d,t, and ^{3}He.

assay was done using a thermal ionization mass spectrometry (TIMS) [11]. In order to subtend a large angular range, the second target was shifted to 51 mm closer to the detector array. Unreacted beam particles were continuously monitored by a graphite beam stop which was located at the downstream side of the target chamber to monitor the beam current during the runs. A 9.5 mm-thick aluminum plate with a collimating aperture (19 mm diameter) was installed upstream of the target position to protect the delicate silicon detectors from being exposed to the intense proton beam.

Recoiling α particles from the ^{24}Mg$(p,\alpha)^{21}$Na reaction were detected by a silicon detector array (SIDAR) [12] which was composed of four trapezoidal wedges of ΔE-E telescopes. The detector wedges were tilted 43° from the perpendicular to form a "lamp-shade" configuration for a large angular acceptance. Each telescope was constituted with a 100 μm-thick (ΔE) detector backed by a 1000 μm-thick (E) detector. The angles subtended by SIDAR were $17^\circ < \theta_{\rm lab} < 44^\circ$ ($19^\circ < \theta_{\rm c.m.} < 50^\circ$) for one target position and $24^\circ < \theta_{\rm lab} < 63^\circ$ ($27^\circ < \theta_{\rm c.m.} < 70^\circ$) for the other. By using highly segmented silicon strip detectors, the differential cross sections of the reaction could be measured at multiple angles simultaneously.

The energy response of each silicon strip was calibrated by using an α-emitting source composed of ^{237}Pu (5.157 MeV), ^{241}Am (5.486 MeV), and ^{244}Cm (5.805 MeV). The energy offset of each analog-to-digital convertor (ADC) channel was also obtained by using the α peaks at the three energies. An additional calibration was performed by using a calibrated ^{244}Cm source to measure the solid angle subtended by each strip.

Light charged particles from the reactions were identified by standard energy loss technique. A typical particle-identification plot obtained at $\theta_{\rm lab} = 27.2^\circ$ ($\theta_{\rm c.m.} = 30.4^\circ$) is shown in Fig. 2. The α yields (i.e., the events falling in the red gate) were clearly identified as shown in the figure with no evidence of contamination from other charged particle groups such as p, d, t, and ^{3}He.

III. DATA ANALYSIS

A. Internal calibration and excitation energies

The energy spectrum of the detected α particles is displayed in Fig. 3 along with labels of the corresponding ^{21}Na levels. The spectrum was obtained from a strip at $\theta_{\rm lab} = 25.4^\circ$ ($\theta_{\rm c.m.} = 28.4^\circ$) in this case. Twelve peaks were reliably populated at all of the angles covered by SIDAR. The α-energy spectra for each strip of the SIDAR were internally calibrated by using a wide range of well-known energy levels in ^{21}Na from Dubois *et al.* and Fernández *et al.* [13,14], since the recorded ADC channels are not always linearly dependent with the actual energies of incident particles. The internal energy calibrations for ^{4}He energies were performed at each strip of SIDAR by using four strongly populated ^{21}Na energy levels located at $E_x = 0.332$, 2.798, 4.419, and 6.879 MeV which are labeled with asterisks in Fig. 3. The internal energy

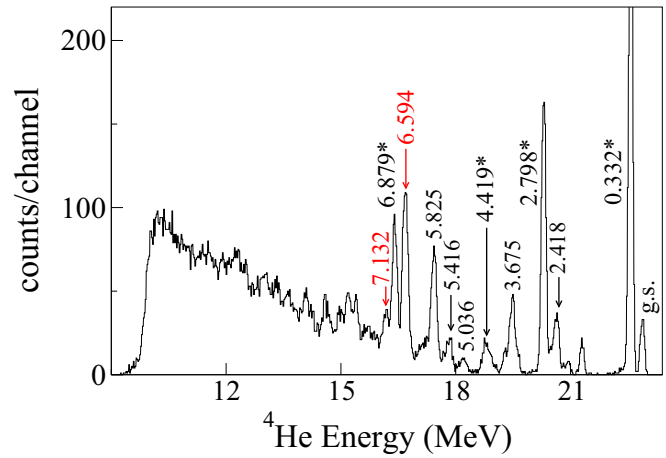

FIG. 3. A typical α energy spectrum obtained at $\theta_{\rm lab} = 25.4^\circ$ ($\theta_{\rm c.m.} = 28.4^\circ$) is shown. The energy levels labeled with asterisks were used for internal energy calibration. Newly observed energy levels are labeled in red. All excitation energies are in MeV.

TABLE I. Excitation energies and J^π values in ^{21}Na extracted from present work and Firestone compilation [18] are summarized. All excitation energies are in keV. Values in parentheses are tentative assignments.

E_x in present work	E_x in Ref. [18]	J^π in this work	J^π in Ref. [18]
0 ± 4	0	$(3/2,5/2)^+$	$3/2^+$
332 ± 1[a]	331.9±0.1	$(3/2,5/2)^+$	$5/2^+$
2418 ± 21	2423.8±0.4	$1/2^+$	$1/2^+$
2798 ± 2[a]	2797.9±0.5	$(1/2,3/2)^-$	$1/2^-$
–	2829.1±0.7	–	$9/2^+$
3675 ± 9	3678.9±0.4	$(1/2,3/2)^-$	$3/2^-$
–	4294.3±0.6	–	$5/2^+$
4419 ± 7[a]	4419 ± 2	$(3/2,5/2)^+$	$(11/2)^+$
–	4467.9±0.7	–	$3/2^+$
5036 ± 11	5020 ± 9	$(3/2,5/2)^+$	$(3/2,5/2,7/2)^+$
–	5380 ± 9	–	$(3/2,5/2,7/2)^+$
5416 ± 17	5457 ± 1	$1/2^+$	$1/2^+$
5825 ± 7	5815 ± 1	$(5/2,7/2)^-$	$7/2^-$
–	5828 ± 1	–	$3/2^-$
–	6468 ± 20	–	$3/2^+$
6594 ± 6	–	$(3/2,5/2)^+$ or $[(1/2,3/2)^- + (7/2,9/2)^+]$	–
6879 ± 3[a]	6879 ± 15	$(1/2,3/2)^-$	$3/2^-$
–	6992 ± 15	–	$7/2^-$
7132 ± 14	–	$1/2^+$ or $(1/2,3/2)^-$	–
–	7253 ± 15	–	$1/2^+$

[a]This level was used for calibration.

calibrations resulted in good agreement in excitation energies obtained from each SIDAR strip at low excitation energies, but larger uncertainties were obtained at higher energies due to the required extrapolation as summarized in Table I. Calibrated ^{4}He energies were then converted to ^{21}Na excitation energies at each angle using known reaction kinematics and detector geometry. The extracted excitation energies assuming each peak arose from a singlet state for ^{21}Na levels are labeled in the figure as well.

The result of internal calibrations shows that two energy levels populated in the present work ($E_x = 6.594$ and 7.132 MeV) do not correspond to any known state in ^{21}Na from the literature. To confirm that the peaks do arise from the ^{24}Mg$(p,\alpha)^{21}$Na reaction, excitation energies were extracted at ten angles by assuming the relativistic kinematics of the ^{24}Mg$(p,\alpha)^{21}$Na reaction. Similar calculations of excitation energies were also performed for the ^{16}O$(p,\alpha)^{13}$N, ^{14}N$(p,\alpha)^{11}$C, and ^{12}C$(p,\alpha)^{9}$B reactions in order to rule out the possibilities that the peaks arose from the contaminations in the target such as ^{16}O, ^{14}N, and ^{12}C. Excitation energies extracted assuming the ^{24}Mg$(p,\alpha)^{21}$Na (black squares) and ^{16}O$(p,\alpha)^{13}$N (red triangles) reactions are shown in Fig. 4 as functions of $\theta_{\text{c.m.}}$ for the 6.594- (top) and 7.132-MeV (bottom) levels. As shown in the figure, the excitation energies are rather consistent for the ^{24}Mg$(p,\alpha)^{21}$Na reaction kinematics, indicating that the peaks did not arise from any contamination in the target. Although the targets are isotopically enriched (99.9%), the possibility that the peaks are originated from the 0.1% isotopes such as ^{25}Mg or ^{26}Mg cannot be completely ruled out. Therefore, the kinematics calculations were also performed by assuming the peaks arose from the ^{25}Mg$(p,\alpha)^{22}$Na or ^{26}Mg$(p,\alpha)^{23}$Na reactions. Results indicate that the two peaks correspond to $E_x =$ 10.368(19) and 10.905(20) MeV in ^{22}Na or $E_x = 11.726(12)$ and 12.262(23) MeV in ^{23}Na, respectively. There are, however, no known energy levels in either ^{22}Na or ^{23}Na at these energies from the literature. Excitation energies extracted for 12 populated levels in the present work are summarized in Table I.

B. Angular distributions and single particle properties

The differential cross sections of energy levels at the center of mass system at each angle θ can be calculated as

$$\left(\frac{d\sigma}{d\Omega}\right)_{j,\theta} = \frac{Y_{j,\theta}}{IN\Delta\Omega_\theta}, \quad (1)$$

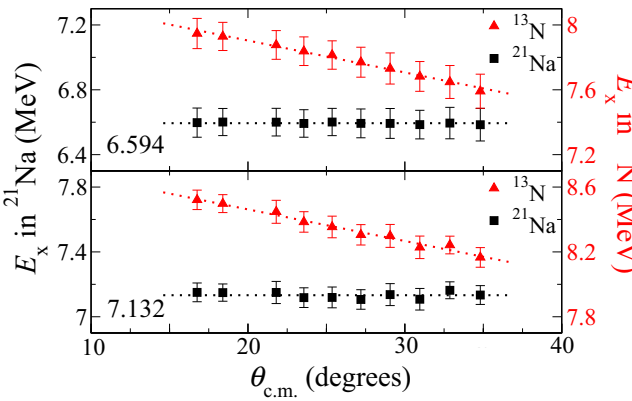

FIG. 4. Excitation energies extracted at ten angles for two newly observed peaks are plotted as functions of $\theta_{\text{c.m.}}$. The average values of excitation energies were determined to be 6.594(6) and 7.132(14) MeV for the peaks, respectively. The black squares (red triangles) represent the calculated excitation energies of ^{21}Na (^{13}N) assuming the peak arose from the ^{24}Mg$(p,\alpha)^{21}$Na [^{16}O$(p,\alpha)^{13}$N] reaction.

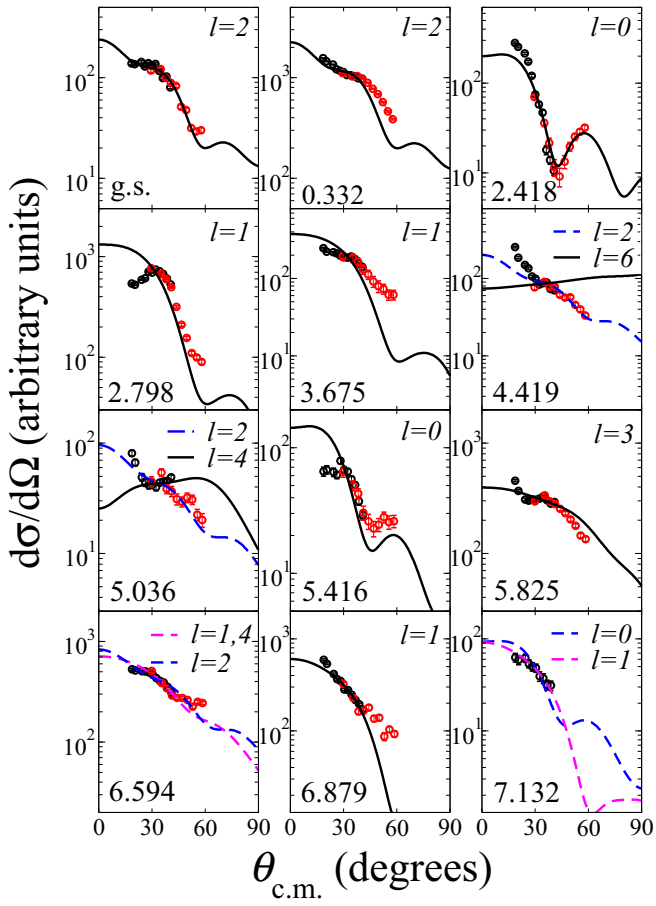

FIG. 5. The angular distributions of α particles from the ^{24}Mg$(p,\alpha)^{21}$Na reaction (circles) for 12 levels are shown. The red and black circles are from the two different target positions, respectively. DWBA calculations for known l transfers are shown as black solid lines. The dashed lines represent the DWBA calculations best fitting the experimental data. All excitation energies are in MeV.

where $Y_{j,\theta}$ is the ^{4}He yield from the ^{24}Mg$(p,\alpha)^{21}$Na reaction for an energy level j, I is the number of beam particles incident on the target, N is the number of target ^{24}Mg atoms per unit area, and $\Delta\Omega_\theta$ is the solid angle subtended by a SIDAR strip in the center of mass system. Due to the large uncertainties in beam current normalization and target stoichiometry, I and N are not included in the cross section calculations. This does not affect the shape of the angular distributions, however, since the yields of α particles were measured at all angles simultaneously. The angular distributions extracted for 12 strongly populated levels are shown in Fig. 5. The black and red circles represent differential cross sections obtained from two target positions. Statistical uncertainties in the cross sections are shown in the figure, but are smaller than the size of the circles in most cases.

In order to constrain the spins and parities of identified levels, the empirical angular distributions were compared with distorted wave Born approximation (DWBA) calculations using the zero range computer code DWUCK4 [15]. The optical model parameters were taken and slightly modified from Refs. [16] and [17] for the ^{24}Mg $+ p$ and ^{21}Na $+ \alpha$ channels, respectively. The parameters used for the exit channel (^{21}Na $+ \alpha$) were originally determined for the ^{20}Ne$(\alpha,\alpha)^{20}$Ne scattering but also resulted in good fits to the extracted angular distributions in the present ^{24}Mg$(p,\alpha)^{21}$Na reaction data. Because the DWBA theory is only valid for the forward angle part of the angular distribution, a set of optical model parameters that can well reproduce the positions (i.e., angles) of the forward maxima obtained from the experiment was chosen. Table II summarizes the optical model parameters used for the calculations. As shown in Fig. 5, DWBA calculations with proper l transfers ranging from $l = 0$ to $l = 3$ well reproduce angular distributions of eight levels having well-known spin and parity assignments [18]: $E_x = 0, 0.332, 2.418$, 2.798, 3.675, 5.416, 5.825, and 6.879 MeV.

An exception is the energy level at $E_x = 4.419$ MeV. The level is known to have $J^\pi = 11/2^+$ previously [19], which corresponds to $l = 6$ transfer in the current work. As shown in Fig. 5, however, the empirical angular distribution of the level was better described by $l = 2$ transfer (blue dashed line) than $l = 6$ one (black solid line), which leads to $J^\pi = 3/2^+$ or $5/2^+$. One of the possible explanations for this discrepancy is that the observed level could be a multiplet, since there are other known energy levels close to the 4.419 MeV level at 4.294 and 4.468 MeV [20].

The results of DWBA calculations for various l values were compared with angular distributions for the three energy levels located at $E_x = 5.036$, 6.594, and 7.132 MeV to constrain the spins and parities of the states. The triton transfer from the $1d_{\frac{5}{2}}$ shell were considered. The spin and parity of the state at 5.036 MeV were constrained to be $3/2^+$, $5/2^+$, or $7/2^+$ previously [21,22], which corresponds to $l = 2$ or 4 transfer in this work. The DWBA calculations show that $l = 2$ transfer (blue dashed line) better fits the extracted angular distribution than $l = 4$ transfer (black solid line) as shown in Fig. 5, which can further constrain the spin to be $3/2^+$ or $5/2^+$. The angular distribution of the newly found 6.594 MeV level is well described by $l = 2$ transfer ($J^\pi = 3/2^+$ or $5/2^+$). Since the spin is constrained for the first time, we also considered a possibility that the level is a doublet. The χ^2 analysis of various

TABLE II. The optical model parameters used for the DWUCK4 code are summarized. The definitions of parameters follow the conventions in Ref. [15]. Reduced charge radius of triton and its diffuseness were assumed to be 1.25 and 0.35 fm, respectively. Imaginary potential, V_I, for each particle is taken from the surface Woods-Saxon potential.

Particle	V_R (MeV)	r_{0R} (fm)	A_R (fm)	V_I (MeV)	r_{0I} (fm)	A_I (fm)	r_{0C} (fm)
p	49.8	1.16	0.15	26	1.16	0.64	1.3
^{4}He	183	1.1	0.846	26.8	0.86	0.85	1.25

combinations of l transfer shows that the angular distribution of the level is also well described by a combination of $l = 1$ transfer (90%) and $l = 4$ transfer (10%). In the case of the 7.132 MeV level, the experimental data are reasonably well reproduced either by $l = 0$ ($J^\pi = 1/2^+$) or $l = 1$ ($J^\pi = 1/2^-$ or $3/2^-$).

C. Astrophysical reaction rate and implication

The ^{17}F$(\alpha,p)^{20}$Ne reaction rate was calculated by using the narrow resonance reaction rate formalism

$$N_A\langle\sigma v\rangle = 1.54\times10^{11}(\mu T_9)^{-3/2}\sum_r(\omega\gamma)_r \times \exp(-11.605E_r/T_9) \quad [\mathrm{cm^3\ mol^{-1}\ s^{-1}}]. \tag{2}$$

Here, μ is the reduced mass of the system in atomic mass units, T_9 is the temperature in units of GK, r is the resonance index, $(\omega\gamma)_r$ is the resonance strength in units of MeV, and E_r is the resonance energy in MeV. Since the proton partial width (Γ_p) is much larger than the α partial width (Γ_α) for the resonances relevant to the ^{17}F$(\alpha,p)^{20}$Ne reaction rate calculation, $(\omega\gamma)_r$ reduces to

$$(\omega\gamma)_r = \frac{2J_r+1}{(2j_F+1)(2j_\alpha+1)}\frac{\Gamma_\alpha\Gamma_p}{\Gamma_{\mathrm{tot}}} \tag{3}$$

$$\approx \frac{2J_r+1}{(2j_F+1)(2j_\alpha+1)}\Gamma_\alpha, \tag{4}$$

where J_r, j_F, and j_α are the spins of the resonance state, ^{17}F, and α particle, respectively. Γ_{tot} represents the total width of the level.

The α partial widths of resonances were calculated as

$$\Gamma_\alpha(E) = \frac{2\hbar}{R_n}\sqrt{\frac{2E}{\mu}}P_l(E,R_n)\theta_\alpha^2, \tag{5}$$

where $R_n = 1.37\times10^{-15}(m_F^{1/3}+m_\alpha^{1/3})$ is the nuclear interaction radius, $P_l(E,R_n)$ is the Coulomb barrier penetrability, and θ_α^2 is the α-reduced width. $\theta_\alpha^2 = 0.018$ was assumed for the energy levels included in the reaction rate calculation as suggested in Ref. [23]. The resonance parameters used in the reaction rate calculations are summarized in Table III.

In order to see the impact of the present work, the ^{17}F$(\alpha,p)^{20}$Ne reaction rate was calculated including 11 energy levels (i.e., all energy levels listed in Table III but the 7.132 MeV level which was first observed in this work) by using resonance parameters deduced from the literature [18]. The result is shown as the black dashed line in Fig. 6. The parameters were then updated by using the spin assignments constrained from the present work, and the newly found energy level at $E_x = 7.132$ MeV was included in the second reaction rate calculation. The result is shown as the red solid line in Fig. 6. A total of 12 energy levels ranging from $E_x = 6.879$–8.135 MeV were considered in the reaction rate calculation. The ^{17}F$(\alpha,p)^{20}$Ne reaction rate from the REACLIB compilation V2.0 [24] is also shown as a blue dotted line in Fig. 6, which was used in the previous sensitivity studies [3,8].

TABLE III. The resonance parameters used for the ^{17}F$(\alpha,p)^{20}$Ne reaction rate calculation are summarized.

E_x in ^{21}Na (MeV)	E_r (MeV)	J^π	Γ_α (MeV)	$\omega\gamma$ (MeV)
6.879	0.318	$3/2^-$	1.07×10^{-15}	7.13×10^{-19}
6.922	0.361	$7/2^-$	9.34×10^{-16}	1.24×10^{-18}
7.132[a]	0.571	$1/2^-$	3.37×10^{-9}	1.12×10^{-12}
	0.571	$1/2^+$	1.63×10^{-9}	5.42×10^{-13}
	0.571	$3/2^+$	1.63×10^{-9}	1.08×10^{-12}
7.253	0.692	$1/2^+$	1.48×10^{-7}	4.93×10^{-11}
7.571	1.01	$3/2^-$	4.32×10^{-5}	2.88×10^{-8}
7.575	1.014	$1/2^-$	4.59×10^{-5}	1.53×10^{-8}
7.609	1.048	$3/2^+$	2.04×10^{-5}	1.36×10^{-8}
7.93	1.369	$5/2^-$	1.48×10^{-4}	1.48×10^{-7}
7.946	1.385	$7/2^-$	1.73×10^{-4}	2.31×10^{-7}
7.96	1.399	$1/2^-$	3.81×10^{-3}	1.27×10^{-6}
8.097	1.536	$3/2^-$	1.17×10^{-2}	7.79×10^{-6}
8.135	1.574	$5/2^+$	4.81×10^{-3}	4.81×10^{-6}

[a]This level is newly observed in the present work.

As stated in the previous section, the spin of the 7.132 MeV level was constrained to be $1/2^+$, $1/2^-$, or $3/2^-$ through the present work. The calculated reaction rate assuming one of the possible spin values was not, however, distinguishable from those assuming the other spin values at this scale. Calculations indicate that the newly updated ^{17}F$(\alpha,p)^{20}$Ne reaction rate (the red solid line in Fig. 6) is a factor of five larger than the previous rate at $T = 0.25$ GK mainly due to the contribution from the new energy level at 7.132 MeV.

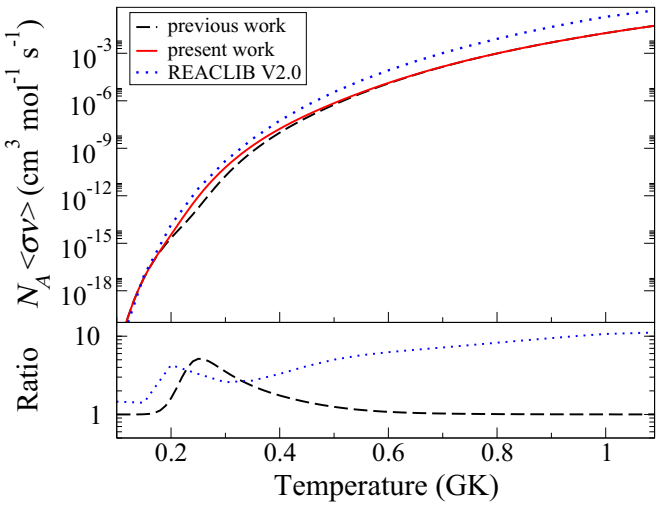

FIG. 6. The ^{17}F$(\alpha,p)^{20}$Ne reaction rate calculated using 11 previously known energy levels in ^{21}Na ranging from $E_x = 6.879$–8.135 MeV is shown as a black dashed line. The contribution from the newly found 7.132 MeV is added to the calculated reaction rate and the result is shown as a red solid line. The ^{17}F$(\alpha,p)^{20}$Ne reaction rate from REACLIB compilation [24] is also shown as a blue dotted line (top). The reaction rate ratio $N_A\langle\sigma v\rangle_{\mathrm{present}}/N_A\langle\sigma v\rangle_{\mathrm{previous}}$ ($N_A\langle\sigma v\rangle_{\mathrm{REACLIB}}/N_A\langle\sigma v\rangle_{\mathrm{present}}$) is also shown in black dashed (blue dotted) line (bottom).

Compared with the $^{17}F(\alpha,p)^{20}Ne$ reaction rate from the REACLIB compilation, however, this newly updated reaction rate is more than a factor of five smaller at $T > 0.4$ GK. In the REACLIB compilation, the $^{17}F(\alpha,p)^{20}Ne$ reaction rate was taken from its inverse reaction, where the stellar enhancement factor was considered [24]. The population of excited states in the target nucleus in the astrophysical plasma was taken into account by considering the stellar enhancement factor. It is therefore possible that the present $^{17}F(\alpha,p)^{20}Ne$ reaction rate is lower than that of the REACLIB compilation. Also, since there might be unresolved levels that are not accounted for by the present reaction rate calculation, our rate could be considered as a lower limit.

IV. CONCLUSIONS

In summary, the $^{24}Mg(p,\alpha)^{21}Na$ reaction was studied to extract spectroscopic information of energy levels in the radionuclide ^{21}Na. By using a 31-MeV proton beam and isotopically enriched ^{24}Mg solid targets, the energies and angular distributions of recoiling α particles from the reaction were measured. A total of 12 energy levels were identified in the energy range of $E_x < \sim 7.2$ MeV, of which two energy levels located at 6.594 and 7.132 MeV were observed for the first time. By comparing the observed differential cross sections with DWBA calculations, we could constrain the following spin and parity assignments: $E_x = 4.419\,\text{MeV} - (3/2,5/2)^+$, $E_x = 5.036\,\text{MeV} - (3/2,5/2)^+$, $E_x = 6.594\,\text{MeV} - (3/2,5/2)^+$, $E_x = 7.132\,\text{MeV} - 1/2^+$ or $(1/2,3/2)^-$. The astrophysical $^{17}F(\alpha,p)^{20}Ne$ reaction rate was also calculated by using 12 energy levels above the α threshold. The calculations indicate that the reaction rate is increased by a factor of five at $T = 0.25$ GK due to the newly observed 7.132 MeV energy level. Although our understanding of the astrophysically important $^{17}F(\alpha,p)^{20}Ne$ reaction rate is considerably improved by the present work, more precise spectroscopic information or direct measurements are required since many resonance parameters had to be estimated in our calculation.

ACKNOWLEDGMENTS

This work was supported by National Research Foundation of Korea (NRF) grants funded by the Korea government Ministry of Education, Science, and Technology (MEST) Nos. NRF-2014S1A2A2028636, NRF-2015R1D1A1A01056918, NRF-2016K1A3A7A09005579, and NRF-2016R1A5A1013277. This research was supported in part by the National Nuclear Security Administration under the Stewardship Science Academic Alliances program through U.S. DOE Cooperative Agreement No. DE-FG52-08NA28552 with Rutgers University and Oak Ridge Associated Universities. This work was also supported in part by the Office of Nuclear Physics, Office of Science of the U.S. DOE under Contracts No. DE-FG02-96ER40955 with Tennessee Technological University, No. DE-FG02-96ER40983 with the University of Tennessee, and No. DE-AC-05-00OR22725 at Oak Ridge National Laboratory, and the National Science Foundation.

[1] P. A. Young *et al.*, Astrophys. J. **640**, 891 (2006).
[2] F. X. Timmes, S. E. Woosley, D. H. Hartmann, and R. D. Hoffman, Astrophys. J. **464**, 332 (1996).
[3] G. Magkotsios *et al.*, Astrophys. J. Suppl. Ser. **191**, 66 (2010).
[4] A. F. Iyudin *et al.*, Astron. Astrophys. **284**, L1 (1994).
[5] J. Vink, Adv. Space Res. **35**, 976 (2005).
[6] W. D. Arnett, J. N. Bahcall, R. P. Kirshner, and S. E. Woosley, Annu. Rev. Astron. Astrophys. **27**, 629 (1989).
[7] S. E. Woosley and R. D. Hoffman, Astrophys. J. Lett. **368**, L31 (1991).
[8] R. H. Cyburt *et al.*, Astrophys. J. **830**, 55 (2016).
[9] S. E. Woosley *et al.*, Astrophys. J. Suppl. Ser. **151**, 75 (2004).
[10] J. G. Pronko *et al.*, Nucl. Phys. A **140**, 465 (1970).
[11] https://isotopes.gov/
[12] D. W. Bardayan, J. C. Blackmon, W. Bradfield-Smith, C. R. Brune, A. E. Champagne, T. Davinson, B. A. Johnson, R. L. Kozub, C. S. Lee, R. Lewis, P. D. Parker, A. C. Shotter, M. S. Smith, D. W. Visser, and P. J. Woods, Phys. Rev. C **63**, 065802 (2001).
[13] J. Dubois, H. Odelius, and S. O. Berglund, Phys. Scr. **5**, 163 (1972).
[14] M. Fernández, G. Murillo, J. Ramírez, O. Avila, S. E. Darden, M. C. Rozak, J. L. Foster, B. P. Hichwa, and P. L. Jolivette, Nucl. Phys. A **369**, 425 (1981).
[15] P. D. Kunz, http://spot.colorado.edu/~kunz/DWBA.html
[16] R. L. Kozub, Phys. Rev. **172**, 1078 (1968).
[17] J. B. A. England, E. Casal, A. Garcia, T. Picazo, J. Aguilar, and H. M. S. Gupta, Nucl. Phys. A **284**, 29 (1977).
[18] R. B. Firestone, Nucl. Data Sheets **127**, 1 (2015).
[19] S. Thummerer *et al.*, J. Phys. G: Nucl. Part. Phys. **29**, 509 (2003).
[20] A. Gade, P. Adrich, D. Bazin, M. D. Bowen, B. A. Brown, C. M. Campbell, J. M. Cook, T. Glasmacher, K. Hosier, S. McDaniel, D. McGlinchery, A. Obertelli, L. A. Riley, K. Siwek, J. A. Tostevin, and D. Weisshaar, Phys. Rev. C **76**, 061302(R) (2007).
[21] R. G. Sextro, R. A. Gough, and J. Cerny, Phys. Rev. C **8**, 258 (1973).
[22] F. X. Haas, C. H. Johnson, and J. K. Bair, Nucl. Phys. A **193**, 65 (1972).
[23] I. Pogrebnyak, C. Howard, C. Iliadis, R. Longland, and G. E. Mitchell, Phys. Rev. C **88**, 015808 (2013).
[24] R. H. Cyburt *et al.*, Astrophys. J. Suppl. Ser. **189**, 240 (2010).